Evaluation of a Range of MRI-Active pH Indicators Using a Multiple-Sample Method

Stephen Evans and Laurie Hall
Herchel Smith Laboratory for Medicinal Chemistry, University of Cambridge School of Clinical Medicine, Cambridge CB2 2PZ, U.K.

DOI 10.1002/aic.10387
Published online March 10, 2005 in Wiley InterScience (www.interscience.wiley.com).

A multisample magnetic resonance imaging (MRI) method was used to measure the effects of a range of paramagnetic metal ions and chelating ligands on the T_1 and T_2 values of the protons of water over the pH range of 2 to 12. Copper sulfate and manganese chloride were combined with one or more of the following chelating agents:- ethylenediamine, ethylenediaminetetraacetic acid, diethylenetriaminepentaacetic acid, ethylene glycol-bis-tetraacetic acid, D-penicillamine, or triethylenetriamine; Gd(III)DTPA was used as purchased. The multisample MRI method was also used to determine the sensitivity of aqueous MnEDTA to pH of carrots to demonstrate how the medium under investigation causes an offset to the calibration acquired in vitro. That calibration enabled null-point T_1 imaging and maps of T_2 values to track the change in pH as acetic acid diffused into the carrot tissue. © 2005 American Institute of Chemical Engineers *AIChE J,* 51: 1541–1547, 2005
Keywords: pH, MRI, diffusion, mass transfer, food

Introduction

The ability to measure pH is fundamental to the control of numerous processes in chemistry and biology. Although conventional methods for measuring pH, which have traditionally included titration and electrical probes, can be extremely accurate, they are generally invasive, thereby destroying or altering the process under investigation. Importantly, they provide little or no information about the spatial or temporal heterogeneity of a process; this current lack of understanding limits the optimization of many processes and can result in wastage of materials, time and energy. Hence, there is a need for an analytical method that is noninvasive and nondestructive and which has good temporal and spatial resolution; one such method that could fulfil these requirements is magnetic resonance imaging (MRI). Although pH cannot generally be measured directly by MRI, this study demonstrates that the chemical potential of a system can be 'probed' noninvasively using "MR-active chemical indicators."

A "molecular amplifier" is a substance which at high dilution significantly influences the magnetic resonance (MR) properties of the protons of water or lipids; its "gain" can be controlled by varying either its chemical or magnetic properties. If the "gain" of that amplifier is sensitive to the chemical potential of its molecular environment, then it can be used as an "MR-active indicator of chemical potential" via spin-spin coupling[1] or by its effects on the relaxation times of the protons of water.[2,3,4] For example, Magnetic resonance spectroscopy (MRS) can measure pH using molecules with pH sensitive resonances, such as those of ^{31}P[5,6,7] ^{13}C[8] or ^{19}F.[9,10] It is also possible to use novel MRS pulse sequences to detect very low and otherwise undetectable resonances from NH protons that are typically in fast exchange with water solvent.[11,12]

However, in order to map the spatial distribution of pH it is necessary to exploit the ^{1}H nucleus since it offers the highest sensitivity. For example, it is possible to image the spatial distribution of pH *in vivo* using magnetic resonance spectroscopic imaging (MRSI) in combination with imidazole, due to the pH sensitive resonance of the protons on the C-2 carbon in the imidazole ring.[13,14,15] MRS and MRSI techniques have the advantage that the measurement is independent of the concentration of the pH probe, but compared to MRI, they have a lower spatial resolution.

With MRI, it is possible to measure extracellular and intracellular pH using pH-sensitive gadolinium complexes and gadolinium containing pH sensitive polyion complexes[13,16–25]. For

Correspondence concerning this article should be addressed to L. D. Hall at ldh11@hslmc.cam.ac.uk

nonclinical applications the simplest way to map pH is via the relationship between metal ion solubility and pH; the presence of more, or less, paramagnetic material in aqueous solution causes an inversely proportional change in the observed nuclear relaxation times of the water protons.[26] Alternatively, metal ions can be chelated with ligands that bind to the metal ion depending on the pH. For chelated metal ions, the variation of relaxation times of water protons with pH does not rely on precipitation of the paramagnetic species. Instead, multidentate ligands form protonated or mixed complexes with hydroxides, which alter the access of water to the paramagnetic core. At extreme pH values, ligand protonation and metal hydroxide formation are major drivers for the dissociation of metal complex.[27,28] Thus, the relaxivity of the solvent protons varies with pH which, in simple cases, can be simulated and put to use as NMR active pH indicator.[29] In principle, the large number of possible combinations of ligands and paramagnetic metal ions could provide a specific indicator to cover individual sectors of the entire pH range.[26] The optimal pH range of a particular indicator can be fine-tuned toward lower pH values by adding excess ligand.[30] The indicator range can also be altered by the addition of competing ligands and diamagnetic cations; for example, depending on the pH, the addition of small monodentate ligands can replace residual co-ordinated water,[27] or destabilize the metal chelate.[31]

The prediction of the pH-sensitivity of a specific combination of metal ion and ligand requires knowledge of the molar relaxivities of each species and of the formation constants of the complexes involved. The latter can be taken from the literature[32,26] as can some values for molar relaxivity of metal ions.[33,34]

The indicators chosen for this study used the paramagnetic ions, manganese (II), copper (II) or gadolinium (III) in combination with the ligands ethylenediaminetetraacetic acid (EDTA), ethylenediamine (en), diethylenetriaminepentaacetic acid (DTPA), ethylene glycol-bis-tetraacetic acid (EGTA), D-penicillamine (Pen) or triethylenetriamine (Tri). In principle, those metal-ligand combinations should cover a wide range of pH values.

It has been previously demonstrated that null-point MRI imaging can be used to visualize and measure the change in pH associated with sulfuric acid diffusing through polyacrylamide gels doped with Cu EDTA.[35,36,37] A range of indicators for mapping a pH range of 3 to 5 in food systems has also been developed.[38] However, for future applications, it is important to develop pH indicators for the entire pH range; that development requires evaluation of an almost limitless combination of metal ions and ligands and of environments in which to use these indicators. Using conventional bulk MR methods that enable only one sample to be placed in the magnet at one time could make such evaluations very time-consuming. Instead, we propose to use a more efficient multiple-sample MRI method[39] to enable large numbers of samples to be measured in a single imaging session. This study demonstrates that approach to determine the pH sensitivity of 11 different metal-ligand combinations via measurements of both the spin-lattice (T_1) and spin-spin (T_2) relaxation times of the protons of the water solvent.

However, it is important to note that molar relaxivities are affected by the particular system under investigation and they need to be determined for each environment.[40,41,42] Hence, once the general sensitivity of a particular metal-ligand combination has been determined *in vitro*, a specific calibration has to be made for each specific system of interest. Again, the multiple-sample method can be used efficiently to determine that calibration curve. In this study, an example is given of tracking changes in pH during the pickling of carrots via null-point T_1 imaging, which was developed using the multisample approach.

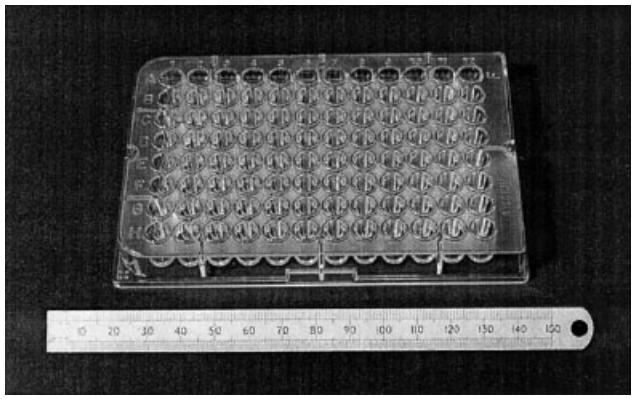

Figure 1. Multiwell plate containing 8 by 12 wells (96 wells in total).

Materials and Methods

MRI hardware

All images were acquired at room-temperature (ca. 22°C) using a 2.35 Tesla 31 cm, horizontal bore superconducting magnet, connected to a Bruker BMT imaging console (Bruker Medzintechnik Biospec II, Karlsruhe, Germany). A 9.4 cm i.d radiofrequency (RF) probe was based on a cylindrical eight strut "birdcage" design operating in quadrature mode inside a 16 cm i.d. gradient set. All gradient sets and RF probes were built "in-house."

Experimental protocol

Each well counter plate (Sterilin, Ltd., UK) was trimmed from 12 by 8 wells (Figure 1) to an array of 6 by 5 wells, each of which could contain 0.5 cm^3 of an MRI-indicator solution. Magnetic susceptibility effects which would have been caused by the air gaps between adjacent wells were eliminated by filling the spaces with 2% (w/v) agar gel doped with 5 mM $MnCl_2$, which reduced the relaxation time of the water protons in the gel so that their contribution to the total MRI signal was negligible. It also improved the ease with which the automated software located the wells within the images.

The magnetic resonance parameters were acquired sequentially from each multi-well plate. The four well plates were stacked vertically in the probe (*y*-axis) and oriented so that five wells were aligned along the bore of the magnet (*z*-axis) with six wells oriented horizontally (*x*-axis). All images had a field of view of 70 mm, 4 mm slice thickness, 128 pixels in the read direction (*z*-axis) with a field of view extension factor of four, and a phase reduction of two; this gave images with 512 by 64 pixels which were later processed to give 128 by 128 pixels with a resolution of 0.547 mm per pixel. That protocol was chosen to give the optimum pixel resolution and signal-to-noise

ratio (SNR of approximately 150) necessary for the automated image analysis, with the minimum time for the full acquisition of the MR parameters.

Data Acquisition

T_1 and T_2 images were acquired from the plates by varying the repetition (TR) and echo time (TE) in the multiecho Carr Purcell Meiboom Gill MRI sequence (43). T_1 values were calculated from images with TR values of 100, 200, 300, 400, 500, 750, 1,000, 1,250, 1,500, 1,750, 2,000, 2,500, 5,000, 7,500, 10,000 ms. T_2 values were quantified by varying TE (16 images, inter-echo time of TE 12, 24, 36, 48, 60, 72, 84, 96, 108, 120, 132, 144, 156, 168, 180, 192 ms, TR 10,000ms). Total image acquisition time was ca. 71 min for T_2 and T_1 images.

The raw data were transferred from the Bruker Aspect 3000 computer via a fast data transfer board (designed by A.A. Wilkinson and Dr. N. Dillon) to a Unix workstation. The image data were zero-padded in the phase direction, base line corrected and a Gaussian filter applied before Fourier transformation. The fitting of the data was performed using a curve-fitting program written by Dr. J. J. Attard and visualized using image display software "Cmrview" written by Dr. N. J. Herrod in the Herchel Smith Laboratory.

Equations 1 and 2 were used to quantify the T_1 and T_2 rates, respectively

$$M_{xy} = M_0\rho(1 - e^{(-T_R/T_1)}) \tag{1}$$

$$M_{xy} = M_0 e^{(-T_E/T_2)} + C \tag{2}$$

where M_{xy} is the magnetization at a particular pixel, ρ and C are the average noise in the images, and M_o, T_1 and T_2 are initial estimates for starting points in the curve-fitting process, which is based on the Levenberg-Marquardt method (44). M_o was quantified by back-projection of the T_2 decay curve to where it intersected the *y*-axis at time zero.

The T_1 and T_2 data for each pH indicator were also normalized using Eq. 3 to enable the sensitivity of a particular pH indicator to be more clearly seen compared to plotting actual T_1 and T_2 values against pH (30)

$$\frac{R_{\text{obs}} - R_{\text{min}}}{R_{\text{max}} - R_{\text{min}}} \tag{3}$$

where R_{obs} is the observed relaxation time and R_{min} and R_{max} are the minimum and maximum relaxation time for a particular pH indicator.

Automatic edge detection

Estimation of the mean values of the MR parameters for each well was achieved by a fully automated computerized analysis. The location of the circular boundaries of the wells was determined by an edge-detection program based on a recursive filtering algorithm originally developed for automated measurements of the thickness of finger joint cartilage.[45] The development of this technique for delineating multiwell plates has been previously demonstrated.[39]

Table 1. List of MR-Active Indicators Investigated

Acronym	Indicator Composition
MnEDTA	0.25 mM MnCl + 0.25 mM Ethylenediaminetetraacetic acid (EDTA)
MnEDTA	0.4 mM MnCl + 0.4 mM Ethylenediaminetetraacetic acid (EDTA)
MnDTPA	0.4 mM MnCl + 0.4 mM Diethylenetriaminpentaacetic acid (DTPA)
Mn(Pen)	0.4 mM MnCl + 0.4 mM Penicillamine (Pen)
Mn(Tri)	0.4 mM MnCl + 0.4 mM Triethylenetriamine (Tri)
Mn(en)	0.4 mM MnCl + 0.4 mM ethylenedimine (en)
CuEGTA	2 mM $CuSO_4$ + 2 mM ethylene glycol-bis-tetraacetic acid (EGTA)
Cu(en)	2 mM $CuSO_4$ + 2 mM ethylenediamine (en)
Cu(Tri)	2 mM $CuSO_4$ + 2 mM Triethylenetriamine (Tri)
CuDTPA	2 mM $CuSO_4$ + 2 mM Diethylenetriaminetetraacetic acid (DTPA)
GdDTPA	2 mM GdDTPA + 2 mM Diethylenetriaminpentaacetic acid (DTPA)

pH Indicators

Eleven different combinations of metal ion and ligand were investigated (Table 1). The samples were taken from a titration of the indicator solution with suitably diluted acid or base (0.05 M sulfuric acid, 0.1 M sodium hydroxide). Since the diluting acid (or base) had the same concentration of metal ion and ligand, the concentration of each MRI indicator was kept constant. The pH was adjusted in approximately 0.5 pH units and a small sample transferred from the solution to the multiwell plates with a pipette. The pH of all samples was measured with a digital pH/mV meter (Ciba Corning Diagnostics, Sudbury, U.K.) using a combination glass electrode (Russel, Auchtermuchty, Scotland) which was calibrated with standard buffers, pH 7, 4 and 2 (BDH, Poole, U.K.) and appropriate temperature correction via an auxiliary temperature sensor. All chemicals were supplied by Sigma-Aldrich, U.K.

pH mapping in carrots

Carrots were obtained fresh from a local market and sliced into sections of approximately 1 cm^3. Manganese chloride was combined with ethylenediamenetetraacetic acid (EDTA) in a ratio of 1:1 at a concentration of 0.2 mM. That indicator solution was formulated in 1 L volumetric flasks, and the pH adjusted to make the solution acidic (pH 1.9) by the addition of 5 cm^3 1 M sulfuric acid, or alkaline (pH 12.2) with 10 cm^3 1 M sodium hydroxide. Sodium azide (0.01 M) was added to the solutions to prevent microbiological spoilage.

The pH was adjusted by titrating the acidified solution with the alkaline solution into a glass jar (*ca.* 200 cm^3 capacity) that was constantly mixed by a magnetic stirrer. A new glass jar was used for each value from pH 6 to 2 in ca. 0.25 pH units, giving 16 different pH values. The pH was measured with a pH electrode (phase electrode, Merck, U.K.) and meter (Model No. 220, Corning, USA); at each incremental change in pH, three sections of carrot were placed into the glass jars. The samples were then left for 2 days at ca. 20 °C, and then the pH of each solution was again measured prior to placing the carrot sections into multiwell plates. The same MRI protocol detailed above was then used to acquire T_1 and T_2 images; the average T_1 and T_2 values for each carrot section was determined by manually

Table 2. Effects of pH on T_1 and T_2 Values

Indicator	Change in T_1 (msec)	pH Sensitivity via T_1	Change in T_2 (msec)	pH Sensitivity via T_2
MnEDTA	660–1340	3.5–5.5	60–380	3.5–5.5
MnEDTA	239–540	3.5–5.5	25–158	3.5–5.5
MnDTPA	241–586	4–6	24–190	4–6
Mn(Pen)	315–1615	6–8	26–780	7–8, 10–11
Mn(Tri)	356–3400	2–9	25–900	6–9
Mn(en)	530–3000	2–9	50–700	8–9.5, 11–12
CuEGTA	800–1750	6–8		
Cu(en)	550–1700	4–6, 7–10		
Cu(Tri)	550–1500	2–6		
CuDTPA	500–1950	3.5–6, 8–9		
GdDTPA	475–1000	2–3.5		

drawing a mask around each section using "Cmrview" software.

From the calibration between T_1 and pH, or T_2 and pH, it was possible to determine the T_1 or T_2 value associated with a particular pH value in the carrot tissue. The T_1 calibration was used to determine the inversion time (τ) of an inversion recovery scan protocol (Eq. 4) so that any pixels with a T_1 value associated with a pH value of 3 will have no signal

$$\tau = T_1 \log_e(2 - e^{-TR/T_1}) \quad (4)$$

where *TR* is the repetition time.[40]

Once the calibrations between pH and MR parameters had been determined, sections of carrot were soaked in 0.2 mM MnEDTA at pH 7 for 2 days. The labeled carrot sections were then immersed in 5% acetic acid (v/v) that had also been doped with the same MRI-indicator, just prior to starting the image acquisition. The MRI scanner was programmed to acquire null-point T_1 images and then T_2 maps from the same carrot section every 30 min during the diffusion of the acetic acid; FOV 30 mm, 3 mm imaging slice thickness, 128 pixels in the read axis and 64 phase encode steps, TR of 2100 ms, TE 10 ms, τ 270 ms for null-point images; TR 2200, TE 12 ms, 16 echo images (interecho time 12 ms) for T_2 images. The images were subsequently processed to give images 128 by 128 pixels with a resolution of 0.234 mm per pixel. Maps of T_2 values were determined using Eq. 2. Time for image acquisition was ca. 5 min for the null-point T_1 image and ca. 5 min for the T_2 images.

Results and Discussions

Table 2 summarizes the T_1 and T_2 values associated with the change in pH values. The sensitivity of each indicator, defined by the slope dT_1/dpH, is dependent on the difference between the molar relaxivity of the two indicator forms present at the two extremes of the useful indicator range. In general, this means that the useful pH range of all indicators was approximately two units. However, for Cu(en) and CuDTPA, there is an additional sensitivity to pH values between 7 and 10; this is because ethylenediamene and DTPA undergo further complexation at higher pH levels, which causes T_1 values to decrease as the pH increases above pH 7. With MnPen and Mn(en), there is also a dual sensitivity, with a sensitivity to pH ranges of 7-8 and 10-11 for MnPen and 8-9.5 and 11-12 for Mn(en), but for these there is no protonation at higher pH levels as T_1 (and T_2) values continue to increase above pH 7.

The only indicators that showed a change in T_2 values with pH were those based on manganese ions (Figure 2a), of which MnTri gave the largest change in T_2 values (ca. 35 fold difference). MnPen followed by Mn(en) also had a large dynamic range (ca. 32 and 28 fold difference, respectively). Although, MnEDTA and MnDTPA did not give such a large change in T_2 values, they still gave a useful 6 – 8 fold change in T_2 values.

Figure 2b demonstrates that by normalizing the T_2 values the pH sensitivity of the indicators based on manganese is more apparent. For the indicators used in this study, manganese ions have a pH sensitivity ranging from pH 3 – 12. Mn(en) and MnPen are unusual in that there is a "plateau" of about 2 pH units where the T_2 values do not change and they have two sensitive pH ranges (Figure 2b).

Compared to T_1 mapping, the ability to map pH via T_2 imaging could enable the measurement of pH values with very good temporal and spatial resolution. T_2 mapping would also

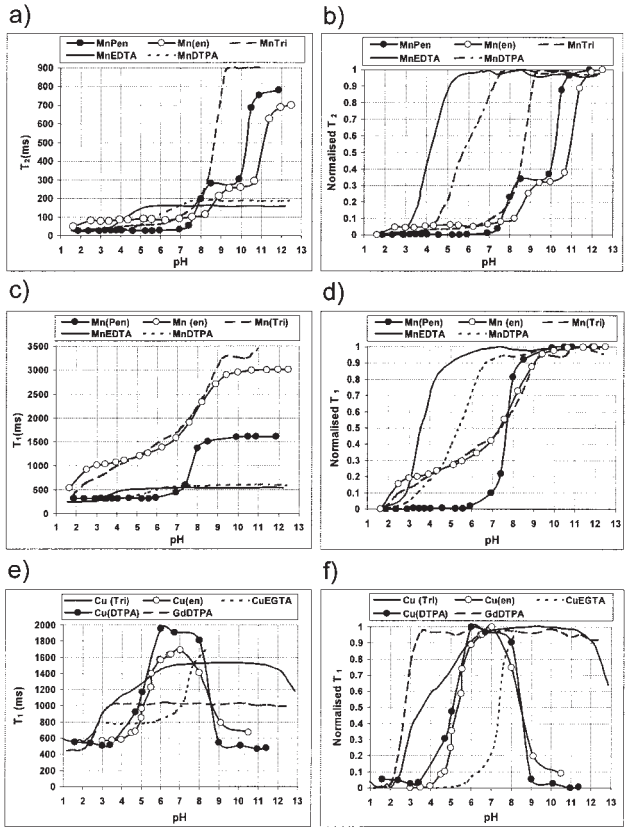

Figure 2. (a) Effect of pH on T_2 values using MnEDTA, MnDTPA, MnTri, MnPen and Mn(en) in vitro; (b) Normalized T_2 values from MnEDTA, MnTPA, MnTri, MnPen and Mn(en); (c) Effect of pH on T_1 values with MnEDTA, MnDTPA, MnDTPA, MnTri, MnPen and Mn(en) *in vitro*; (d) Normalized T_1 values from MnEDTA, MnDTPA, MnTri, MnPen and Mn(en); (e) Effect of pH on T_1 values with CuEDTA, CuDPTA, Cu(en), CuEGTA and GdDTPA; and (f) Normalized T_1 values from CuEDTA, Cu(en), CuTri, CuEGTA and GdDTA.

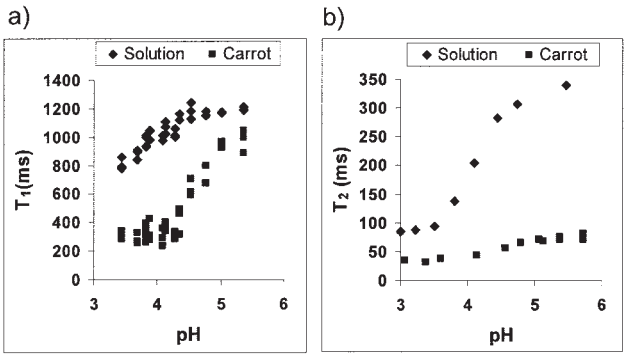

Figure 3. Effect of pH on T_1 values (a) and T_2 values (b) with 0.2 Mm MnEDTA in carrot tissue and in vitro.

enable the measurement of a range of pH values in one image, rather than the visualization of one specific pH value via an optimized null-point T_1 imaging protocol.

For manganse ions, the change in T_1 values associated with changes in pH is not as large as that for T_2 values; MnTri and Mn(en) gave the biggest difference (ca. 9 fold), followed by MnPen (ca. 5 fold) both of which are far smaller than the differences observed in T_2 values for the same pH ranges. MnEDTA and MnDTPA only gave a two-fold difference in T_1 values between pH 3 and 5 compared to ca. 6 to 8 fold difference in T_2 values. Again, normalization of the T_1 values enables the pH sensitivity of indicators, based on manganese ions to be more clearly demonstrated (Figure 2d). Compared to the pH sensitivity observed with T_2 values, the dynamic range of pH values with T_1 is slightly different, with a useful pH sensitivity from pH 2 – 9.

Indicators based on copper or gadolinuim ions also gave a wide range of sensitivities to pH vs. T_1 values. As can be seen in Figure 2e, CuDTPA gave the biggest change (ca. 4 fold difference) followed by Cu(en), CuEGTA, CuTri, and then GdDTPA. For CuEGTA, the chelating agent becomes increasingly insoluble above pH 8. The normalized T_1 results in Figure 2f show that for these indicators, there is a pH sensitivity from pH 2 - 10.

These results are for metal-ligand combinations in aqueous solutions. In order to use these indicators in heterogeneous systems, it is necessary that a calibration be carried out for each combination of the indicator and the system of interest. Fortunately, the multisample method enables the determination of those calibrations to be made very efficiently. To illustrate how important it is to do this calibration and to demonstrate how the multisample method was used to determine this calibration, we present an example of MnEDTA as a pH indicator in carrot tissue. That indicator was selected as it is the best indicator for the pH range of 3 to 5 (Figure 2e) to correspond with the pH of diluted acetic acid (pH 3). It can be seen in Figure 3a that there was a difference in the calibrations between T_1 and pH *in vitro* compared to that in carrot tissue. Similarly, Figure 3b shows that there was also a difference in the calibrations between T_2 values and pH for carrot compared to *in vitro*. Once these calibrations had been determined, it was possible to optimize a T_1 inversion recovery scan protocol so that the null-point corresponded with a T_1 value of 250 ms, or pH 4. The null-point can be seen as a dark band in the carrot tissue that moves into the carrot section (Figure 4). The time taken for the null-point to pass to the center of the carrot was about 15 h; hence it took about 15 h for the pH of the entire carrot to reach a pH value of 4. Close examination of the null-point images in Figure 4 also reveal that the diffusion of the acid is not uniform across the carrot section; it appears to diffuse faster through the inner cortical tissue of the carrot root.

Figure 4 also shows the corresponding T_2 maps alongside the null-point T_1 images. The use of T_2 maps to measure pH is a potentially more powerful method than null-point imaging as it enables a range of pH values to be measured in one image, rather than just one pH value. Although it would appear in Figure 4 that the T_2 values have become uniform after 9 h, there is in fact a distribution of T_2 values that are not clearly revealed in the greyscale images.

The example of acetic acid diffusion into carrot sections demonstrates that MRI could be a potential tool for ensuring the microbiological safety of foodstuffs. Once the basic science of the spatial heterogeneity of any process is understood, the current high cost of MRI could be reduced for subsequent applications by using a low-cost, "bench-top" MR instrument to acquire "bulk" MR measurements. Alternatively, MRI could be used to gain a better understanding of a process and that information then used to develop mathematical models for subsequently industrial scale-up. If the process under study

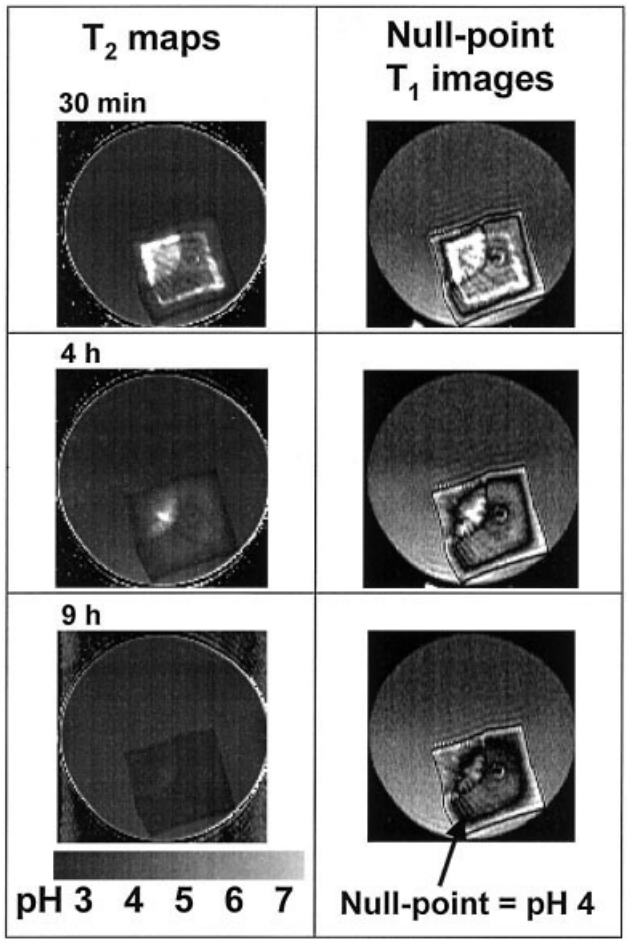

Figure 4. T_2 maps and null-point T_1 images of carrot tissue during the diffusion of acetic acid.

involves friable, opaque materials that change in time and space, then MRI is uniquely the only analytical tool available.

Conclusions

This study has demonstrated that there are a variety of chelate complexes of paramagnetic metal ions which are suitable as MRI indicators for measuring a range of pH values. Importantly, the automated multisample MRI methodology used in this study enabled a survey of different metal ion complexes to be made efficiently and quickly. That same method has also been used to determine the effect of different environments on the calibration of those indicators and to develop novel applications for pH mapping. In this study, null-point imaging of acetic acid diffusion into carrot is given as an example of how pH may be measured using MRI-active pH indicators. The disadvantage of null-point imaging is that only one pH value can be tracked in each experiment. From the survey of indicators carried out, it is clear that those using manganese ions provide the possibility of mapping pH values in two and three dimensions via MRI measurements of the spatial distribution of T_2 values with good spatial and temporal resolution in systems which are friable. The number of samples that can be measured with the multisample method is only limited by the B_1 homogeneity of the magnet.

Acknowledgments

The authors wish to thank the late Dr Herchel Smith for his endowment of HSLMC and the EPSRC for providing additional funding for this study (Grant No. GR/M67346).

Literature Cited

1. Moore GJ, Silerud LO. The pH dependence of chemical shift and spin-spin coupling for citrate. *J Magn Reson*. 1994;103:87-88.
2. Aime S, Botta M, Ermondi G, Fasano M, Terreno E. Paramagnetic water proton relaxation enhancement: from contrast agents in MRI to reagents for quantitative "in vitro" assays. *Magn Reson Imag*. 1992; 10:849-854.
3. Aime S, Fasano, M, Paoletti S, Arnelli A, Ascenzi P. NMR relaxometric investigation on human methoglobin and fluoromethemoglobin. An improved quantitative in vitro assay of human methemoglobin. *Magn Reson Med*. 1995;33:827-831.
4. Fischer AE, Hall LD. Roles for paramagnetic substances in MRI: contrast agents, molecular amplifiers and indicators for redox and pH mapping. *MAG*MA*. 1994;2:203-210.
5. Stubbs M, Bhujwalla ZM, Tozer GM, Rodrigues LM, Maxwell RJ, Morgan R, Howe FA, Griffiths JR. An assessment of 31P MRS as a method of measuring pH in rat tumours. *NMR Biomed*. 1992;5:351-359.
6. Vandenberg JI, Metcalfe JC, Grace AA. Intracellular ph recovery during respiratory-acidosis in perfused hearts. *Am J Physiol.* 1994;266: 489-497.
7. Jayasundar R., Honess D, Hall LD, Bleehen NM. Simultaneous evaluation of the effects of RF hyperthermnia on the intra- and extracellular tumor pH. *Magn Reson Med*. 2000;43:1-8.
8. Nielsen PA, Jaroszewski JW, Norrby P-O Liljefors T. An NMR and ab initio quantum chemical study of acid-base equilibria for conformationally constrained acidic α-amino acids in aqueous solution. *J Am Chem Soc.* 2001;123:2003-2006.
9. Ojugo AS, McSheehy PM, McIntyre DJ, McCoy C, Stubbs M, Leach MO, Judson IR, Griffiths JR. Measurement of the extracellular pH of solid tumours in mice by magnetic resonance spectroscopy: a comparison of exogenous 19F and 31P probes. *NMR Biomed.* 1999;12:495-504.
10. Mason RP. Transmembrane pH gradients in vivo: measurements using fluorinated vitamin B6 derivatives. *Curr Med Chem.* 1999;6:481-504.
11. Mori S., Eleff SM, Pilatus U, Mori N, Van Zijl PCM. Sensitive detection of solvent-saturable resonances by proton NMR spectroscopy: a new approach to study pH effects. *Magn Reson Med*. 1998; 40:36-42.
12. Ward KM, Balaban RS. Determination of pH using water protons and chemical exchange dependent saturation transfer (CEST). *Magn Reson Med.* 2000;44:799-802.
13. Van Sluis R, Bhujwalla ZM, Raghunand, N, Ballesteros P, Alvarez J, Cerdan S, Galous J-P, Ghillies RJ. Imaging of extracellular pH using 1H MRSI. *Magn Reson Med.* 1999;41:743-750.
14. Vermathen P, Capizzano AA, Maudsley AA. Administration and 1H MRS detection of histidine in human brain: application to in vivo pH measurement. *Magn Reson Med.* 2000;43:665-675.
15. Garcia-Martin ML, Herigault G, Remy C, Farion R, Ballesteros P, Coles JA, Cerdan S, Ziegler A. Mapping extracellular pH in rat brain gliomas in vivo by 1H magnetic resonance spectroscopic imaging: comparison with maps of metabolites. *Cancer Res*. 2001;61:6524-6531.
16. Shuter B, Tofts PS, Wang S-C, Pope JM. The relaxivity of Gd-EOB-DTPA and Gd-DTPA in liver and kidney of the Wistar rat. *Magn Reson Imaging*. 1996;14:243-253.
17. Beauregard DA., Parker D, Brindle KM. Relaxation-based mapping of tumour pH. *In: Proceedings of the 6th Annual Meeting of ISMRM, Sydney, Australia*, 1998; 53.
18. Aime S, Botta M, Crich SG, Gioenzana G, Palmisano G, Sisti MA. Macromolecular Gd(III) complex as pH-responsive relaxometric probe for MRI applications. *Chem Commun*. 1998;16:1577-1578.
19. Zhang S, Wu K, Sherry AD. A novel pH-Sensitive MRI contrast agent. *Angew Chem Int Ed*. 1999;21:3192-3194.
20. Mikawa M, Miwa N, Brautigam M, Akaike T, Maruyama A. Gd(3+) loaded polyion complex for pH depiction with magnetic resonance imaging. *J Biomed Mater Res*. 2000;49:390-395.
21. Hovland R., Glogaard C, Aasen AH, Klaveness J. Gadolinium DO3A derivatives mimicking phospholipids; preparation and in vitro evaluation as pH responsive MRI contrast agents. *J Chem Soc*. 2001;2:929-933.
22. Lowe MP, Parker D, Reany O, Aime S, Botta M, Castellano G, Gianolio E, Pagliarin R. pH-dependent modulation of relaxivity and luminescence in macrocyclic Gadolinium and Europium complexes based on reversible intramolecular Sulfonamide ligation. *J Am Chem Soc.* 2001;123:7601-7609.
23. Lokling K-E, Fossheim SL, Skurtveit R, Bjornerud A, Klaveness J. pH-sensitive paramagnetic liposomes as MRI contrast agents: in vitro feasibility studies. *Magn Reson Imaging.* 2001;19:731-738.
24. Lokling K-E, Skurtveit R, Fossheim SL, Smistad G, Henriksen I, Klaveness J. pH-sensitive paramagnetic liposomes for MRI: assessment of stability in blood. *Magn Reson Imaging.* 2003;21:531-40.
25. Raghunand N, Howison C, Sherry AD, Zhang S, Gillies RJ. Renal and systematic pH imaging by contrast-enhanced MRI. *Magn Reson Med.* 2003;49:249-257.
26. Kragten J. *Atlas of Metal-Ligand Equilibria in Aqueous Solution*. Ellis Horwood, Ltd., Chichester, UK; 1978.
27. Schwarzenbach G, Komplexone IX. Titration von metallen mit athylendiamin-tetraessigsaure H4X. Endupunktisindikation durch pH-effekte. *Helv Chim Acta*. 1948;31:459-465.
28. Schwarzenbach G. Cehlatkomplexe des kobalts mit und onhe fremdliganden. *Helv Chim Acta.* 1949;32:839-853.
29. Balcom BJ, Carpenter TA, Hall LD. Spatial and temporal visualisation of two aqueous iron oxidation/reduction reactions by nuclear magnetic resonance imaging. *J Chem Soc Chem Comm RSC*. 1992;4:312-313.
30. Fischer AE. *Novel Applications for NMR Contrast Agents*. PhD Thesis, University of Cambridge; 1996.
31. Ringbom A. The analyst and the inconsistent constants. *J Chem Educ*. 1958; 35:282-288.
32. Ringbom A. *Complexation in Analytical Chemistry*. Interscience, New York, USA; 1963.
33. Lauffer RIB. Paramagnetic metal complexes as water proton relaxation agents for NMR imaging: theory and designs. *Chem Rev.* 1987; 87:901-927.
34. Watson AD, Rocklage SM, Carvlin MJ. *Contrast Agents in Magnetic Resonance Imaging*. Mosby Year Book, New York, USA;1992:372-437.
35. Balcom BJ, Carpenter TA, Hall LD. Spatial and temporal visualisation of a pH-dependent complexation equilibrium by nuclear magnetic resonance imaging. *Can J Chem.* 1992;70:2693-2697.

36. Balcom BJ, Fischer AE, Carpenter TA, Hall, LD. Diffusion in aqueous gelsl; mutual diffusion coefficients measured by one-dimensional nuclear magnetic resonance imaging. *J Am Chem Soc.* 1993;115:3300-3305.
37. Balcom BJ, Fischer AE, Carpenter TA, Hall LD. MRI Measurements of paramagnetic tracer ion diffusion. *Bulletin of Magnetic Resonance*. 1997;18:204-210.
38. Evans SD, Hall LD. MRI indicators for measuring pH and redox in food. In: Webb GA eds. *Magnetic Resonance in Food Science*. Royal Society of Chemistry, MPG Books, UK; 2001:22-28.
39. Evans SD, Nott KP, Kshirsagar A, Hall LD. Efficient magnetic resonance imaging methods for automated quantitation of magnetic resonance parameters from multiple samples. *Magn Reson Chem.* 1997; 35:S76–S80.
40. Fischer AE, Balcom BJ, Fordham E, Carpenter TA, Hall LD. A fast inversion recovery NMR imaging technique for mapping two-dimensions tracer diffusion and dispersion in heterogeneous media. *J Physics D App Phys*. 1995;28:384-397.
41. Fischer AE, Carpenter, TA, Tyler, JA, Hall, LD. Visualisation of mass transport of small organic molecules and metal ions through articular cartilage by Magnetic Resonance Imaging. *Magn Reson Imaging.* 1995;13:819-826.
42. Hall LD, Fischer AE, Nolan MJ, Carpenter TA, Tyler JA. Dynamics of articular joints visualised by MRI: joint Flexion, cartilage-compression and solute-perfusion. *Acta Orthop Scand.* 1995;66:139-141.
43. Meiboom S, Gill M. Modified spin-echo method for measuring nuclear relaxation times. *Review of Scientific Instruments.* 1958;29:688-691 (1958).
44. Marquardt DW. *J Soc Ind Appl Math.* 1963; 11:431-441.
45. Robson MD, Hodgson RJ, Herrod NJ, Tyler JA, Hall LD. A combined analysis and magnetic-resonance-imaging technique for computerised automatic-measurement of cartilage thickness in the distal interphalangeal joint. *Magn Reson Imaging.* 1995;13:709-718.

Manuscript received Mar. 4, 2004, and revision received Aug. 4, 2004.